A Molecular Imprinted PEDOT CMOS Chip-Based Biosensor for Carbamazepine Detection

Abbas Hammoud, *Student Member, IEEE*, Hussein Assaf, Yvon Savaria, *Fellow, IEEE*, Dang Khoa Nguyen, and Mohamad Sawan, *Fellow, IEEE*

***Abstract*—A miniaturized biosensor for carbamazepine (CBZ) detection and quantification was designed, implemented and fabricated. The 1×1 mm^2 CMOS chip was packaged and coupled with a 3-electrode electrochemical cell. A complete characterization of the sensor was conducted via two steps: 1) Molecular imprinting of PEDOT polymer sites by cyclic voltammetry (CV) on glassy carbon electrode (GCE) surfaces; and 2) Quantification of CBZ solutions through both CV, and a current peak detection circuitry. The proposed biosensor offered high-selectivity and high-sensitivity to CBZ molecules. Scanning electron microscopy (SEM) was utilized to validate the synthesis of the PEDOT chains. CBZ removal from the imprinted polymer was conducted through soaking the modified GCEs in acetonitrile (ACN). Extraction was then confirmed by ultraviolet-visible (UV-vis) spectroscopy and CV analyzing data from pre- and post-template extraction. Furthermore, in order to characterize the electrodes' response to CBZ levels in phosphate buffered solution (PBS) with $[Fe(CN)_6]^{3-/4-}$ as a redox pair/mediator, CV and peak detection was conducted resulting in redox peak currents vs. CBZ concentration graphs. The limits of detection (LOD) and quantification (LOQ) were calculated to be 2.04 and 6.2 μg/mL respectively. Finally, selectivity towards CBZ was validated by studying the effect of valproic acid (VPA) and phenytoin (PHT) on the biosensor's performance. The proposed biosensor is highly sensitive and selective to CBZ molecules, simple to construct and easy to operate.**

***Index Terms*—Biosensor, CMOS, electropolymerization, antiseizure medication, carbamazepine, molecular imprinted polymer, PEDOT.**

I. Introduction

EPILEPSY is characterized by recurrent seizures and influences over 50 million patients across the world [1]. Primarily, clinicians prescribe antiseizure medications (ASMs) as a prophylactic treatment. Such ASMs may be taken daily or for protracted periods. Currently, more than twelve ASMs are being utilized. The most common ASM is CBZ, an anticonvulsant which works by blocking presynaptic sodium and calcium voltage-dependent channels [2]. Various side effects of ASMs include dizziness, blurred vision, dysarthria, ataxia, somnolence, and psychomotor slowing.

While treating epileptic patients, clinicians must continuously monitor the levels of CBZ in blood, referred to as Therapeutic Drug Monitoring (TDM). This practice is critical in order to enhance drug dosage, minimize toxicity, eliminate undesirable dug interactions, and ensure proper compliance. Current TDM is conducted via frequent phlebotomy visits, and has several limitations such as: a) drug levels are affected by numerous conditions of which some are unpredictable; b) CBZ levels in blood greatly vary with time of measurement (the levels before taking CBZ are different than after taking the CBZ); and c) going to clinics and waiting for extended periods of time for blood collection is time-consuming, tedious, and may hinder patients from following a strict blood sampling schedule.

Common reported techniques utilized for the detection and quantification of CBZ can be categorized into electrochemical based methods such as CV [3], differential pulse voltammetry (DPV) [4], [5], and amperometry [6], [7], and non-electrochemical based methods such as high performance liquid chromatography (HPLC) [8]–[10], and spectrophotometry [11]. The latter offer the highest sensitivity and selectivity, however, require bulky equipment, trained clinicians, and sample pre-treatment. Furthermore, such methods are cumbersome and cannot be rendered miniature or portable. On the other hand, electrochemical based methods possess great attributes such as sensitivity, speed, low-cost, simplicity, and portability making them good candidates to be utilized in environmental and medical applications. However, contemporary electrochemical based sensors rely on commercially available electrodes that lack selectivity to the target molecules. To the best of our knowledge, no reported miniaturized detection biosensor can selectively measure the CBZ concentration within a complex medium.

Fortunately, MIPs overcome such limitation. They are alternatives to antibodies that are robust, easy to fabricate and could be prepared by various methods. MIPs have been widely coupled with electrochemical techniques improving sensor's selectivity and sensitivity. Liu *et al.*, [12] reports the successful detection of streptomycin residues in food using magnetic MIP based on nanogold-encapsulated poly(o-phenylenediamine) shell on magnetic iron oxide cores. Furthermore, MIPs have been reported for bisphenol A (BPA) detection [13], insecticide

Manuscript received July 14, 2021; revised November 30, 2021; accepted December 15, 2021. Date of publication December 28, 2021; date of current version May 9, 2022. This work was supported by NSERC under Grant CIHR/NSERC CHRP 538852. This paper was recommended by Associate Editor J. Van der Spiegel. *(Corresponding author: Abbas Hammoud.)*

Abbas Hammoud is with the Polytechnique Montréal, Montreal, QC H3T 1J4, Canada (e-mail: abbas.hammoud@polymtl.ca).

Hussein Assaf and Mohamad Sawan are with the Electrical Enigineering, Polytechnique Montréal, Montreal, QC H3T 1J4, Canada (e-mail: hussein.assaf@polymtl.ca; sawan@westlake.edu.cn).

Yvon Savaria and Dang Khoa Nguyen are with the Department of Medicine, Centre Hospitalier de l'Université de Montréal, Montreal, QC H2V2L9, Canada (e-mail: yvon.savaria@polymtl.ca; d.nguyen@umontreal.ca).

Color versions of one or more figures in this article are available at https://doi.org/10.1109/TBCAS.2021.3138942.

Digital Object Identifier 10.1109/TBCAS.2021.3138942

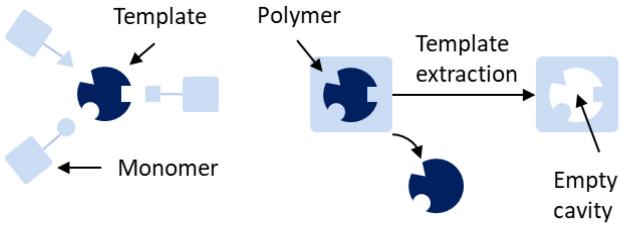

Fig. 1. Molecular imprinting principle.

fenamiphos (FEN) detection [14] ceftizoxime detection [15], epinephrine detection [16], and amyloid-β protein detection [17]. As presented in Fig. 1, a template of interest is chosen to be imprinted within the polymer during the polymerization process. Post-polymerization, the template is extracted from the polymer leaving a gap similar to its structure. Due to the presence of such gaps, the MIP has a high affinity towards the imprinted template. MIPs demonstrated their ability to be vigorous, efficient, and most importantly, inexpensive. Amongst the various methods of MIP synthesis, to date, addition polymerization has been used for CBZ detection. This preparation technique involves a monomer, a cross-linker, a porogen, an initiator along with the template/analyte of interest. Despite their effectiveness, both controlling the thickness of chemically synthesized MIPs and their deposition on the electrodes' surfaces are challenging.

Electropolymerization is an alternative method to synthesize MIPs. It permits the direct formation of controlled thickness MIP layers on the electrode's surface through adjusting the various electrochemical conditions such as monomer concentration, applied voltage, number of cycles, etc. Poly-34-Ethylenedioxythiophene (PEDOT) is a popular biocompatible polymer synthesized by electropolymerization. It has proven to enhance electrodes' sensitivity and fidelity [18]. Additionally, PEDOT has been successfully deployed in nucleic acid detection systems in order to enhance the flexibility of two-dimensional transition-metal carbonitrides $Ti_3C_2T_x$ MXene whilst preserving its conductive properties [19]. Other PEDOT applications are reported in [20] synthesizing a pressure based sensor PEDOT:PSS modified sponge for highly sensitive detection of carcinoembryonic antigen (CEA). PEDOT synthesis requires less time, less skill, and is low-cost compared to additional polymerization.

A biosensor capable of selectively detecting CBZ must consist of an interface circuit connected to specifically modified CBZ sensing electrodes. As part of our previous work, we have reported the development of MIP modified electrodes capable of selectively capturing CBZ molecules overcoming the limitation of miniature electrochemical sensors for CBZ detection [21]. The MIP was based on the electropolymerization of PEDOT on GCEs by CV.

In this paper we present a solution to selectively target CBZ molecules by developing a miniaturized potentiostat-based biosensor capable of the electropolymerization of a PEDOT-based MIP on the biosensing electrodes followed by successive detection of CBZ molecules by CV as shown in Fig. 2. In the remainder of this paper, in section II, we present the

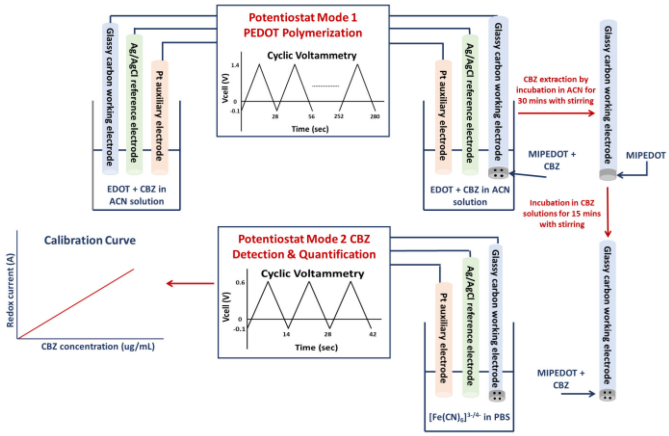

Fig. 2. Proposed sensor's overall design. Mode 1 is for molecular imprinted polymer polymerization, and mode 2 is for CBZ detection and quantification.

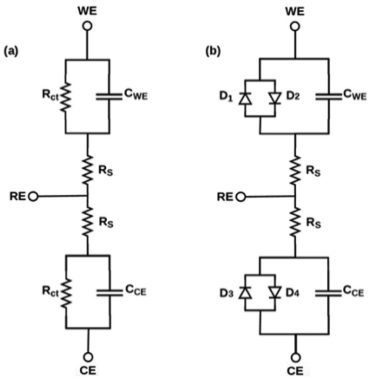

Fig. 3. Electrode-electrolyte interface electrical model. (a) Three-electrode electrochemical cell. (b) Charge transfer resistance replaced by diodes.

electrode-electrolyte model, followed by a system overview analysis and design considerations in Section III. Afterwards, Section IV encompasses post-layout simulations along with results of the fabricated chip and in-vitro experiments. Finally, in Section V we present a conclusion of our work.

II. An Electrochemical Cell

Understanding the electrode-electrolyte interface is crucial to enable design of an effective potentiostat and to simulate accurately its behavior. Fig. 3 presents the adopted electrical model circuit of the electrode-electrolyte interface for the 3-electrode cell. R_s is the solution resistance that exists between combinations of working electrode (WE), counter electrode (CE) and reference electrode (RE).

R_S can be determined by (1), Values of R_S have been reported in the range of 10 to 220 Ω [22].

$$\mathrm{Rs} = \frac{\rho}{4\mathrm{r}} \tag{1}$$

where r denotes the radius of the electrodes and ρ is the resistivity of the solution.

The current path across the electrode-electrolyte interface is represented by a capacitance in parallel with a non-linear

resistance. C_{WE} and C_{CE} are the capacitances at the WE-electrolyte and the CE-electrolyte interfaces respectively. The Gouy-Chapman-Stern model (GCS) offers a derivation of the interface capacitance as a series combination of the double layer capacitance, known as the Helmholtz capacitance C_H, and the diffusion layer capacitance, known as the Gouy-Chapman capacitance C_G. This theoretical derivation is determined by (2). Depending on different electrolyte compositions and modifications to the WE surface, [22], [23] report the values of C_{WE} in the order of 1 to 100 μF cm^{-2}.

$$\frac{1}{C} = \frac{1}{C_H} + \frac{1}{C_G} = \frac{d_{OHP}}{\varepsilon_0 \varepsilon_r} + \sqrt{\frac{\varepsilon_0 \varepsilon_r U_t}{2n^0 z^2 q}} \cdot \frac{1}{\varepsilon_0 \varepsilon_r \cosh\left(\frac{z\phi_0}{2U_t}\right)} \tag{2}$$

where d_{OHP} and ε_r are the double layer's thickness and relative permittivity respectively. ε_0 is the permittivity of free space, z is the solution's ion charge, ϕ_0 is the applied potential, U_t is the thermal voltage, q is the elementary charge, and n^0 is the concentration of ions in the bulk solution.

The non-linear resistance depends on several mechanisms such as the charge transfer at the electrode's surface, the chemical reactions and the diffusion of reactants to and from the electrode's surface along with the crystallization process. However, both the crystallization process and chemical reactions may be ignored. Therefore, this resistance is mainly due to the charge transfer resistance represented by R_{ct} and can be determined by (3).

The resistance R_{ct} has been reported to range between 1 and 10 MΩ [24]. This resistance decays exponentially to a couple of kΩ at large overpotentials, and could be replaced by two diode-connected MOSFETs in reverse parallel as shown in Fig. 3(b).

$$R_{ct} = \left(\frac{V_t}{J_0 z}\right) \frac{1}{\cosh\left(\frac{z\eta}{2V_t}\right)} \tag{3}$$

In (4), J_0 is the absolute value of the oxidation and reduction current at equilibrium, η is the overpotential, $V_t = kT/q$ which denotes the thermal voltage, $\Delta\psi_0$ denotes the equilibrium potential, β denotes the symmetry factor, k_c denotes the reduction reaction rate constant, and c_A denotes the electron-acceptor ions' concentration.

$$J_0 = F k_c c_A e^{\frac{\beta \Delta \psi_0}{V_t}} \tag{4}$$

III. System Overview

Fig. 4 presents the architecture of a basic 3-electrode potentiostat cell. It consists of a control amplifier followed by a current to voltage converter circuit. The core function of the potentiostat stems from the regulation of the WE node potential to match the RE node potential, while measuring the current flowing through WE, and ensuring that no current flows into RE.

The applied potential VSource is the same as the potential on RE, since the voltage at both +ve and –ve terminals of the Op-Amp are nominally equal, if the amplifier has a negligible offset. Similarly, since the +ve terminal of the second Op-Amp is connected to Vref, the potential at WE is set to Vref. These

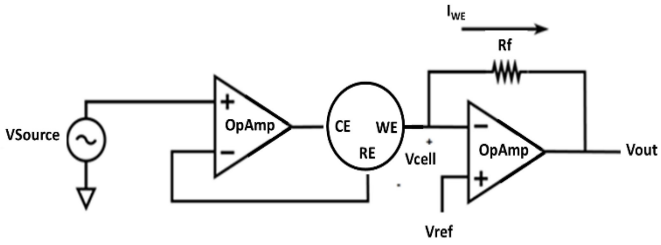

Fig. 4. Basic potentiostat design of a 3-electrode electrochemical cell.

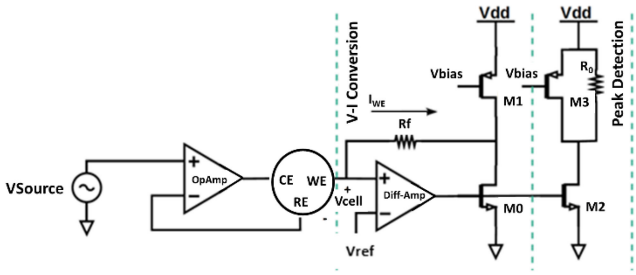

Fig. 5. Proposed potentiostat design with I-V conversion and peak detection circuitry.

two settings enable the regulation of the WE potential to match that on RE.

Given that the Op-Amp's input impedance is high, no current flows through it. Therefore, all the current flows from CE through WE with no current passing through RE. Additionally, the second Op-Amp is utilized to measure the current passing through WE. This current is converted into a potential drop across the feedback resistor Rf. These fundamental functions of the potentiostat necessitate the design of high gain and high input impedance Op-Amps.

The proposed design in Fig. 5 occupies 0.55×0.55 mm^2 chip area and was fabricated in a standard 180 nm CMOS process. It consists of a sensing channel and a control amplifier used to regulate the cell voltage across WE with respect to RE. Additionally, the sensing channel compromises a current to voltage conversion and a peak detection stage. The biosensor detects CBZ molecules through a two-step process. First, by applying a cyclic voltage signal to form the MIP on the electrode's surface, followed by another cyclic voltage signal for CBZ detection. The resulting anodic and cathodic currents yield a proportional voltage that could be measured across the feedback resistance at the transimpedance amplifier stage. On the other hand, the peak detection circuitry detects the peak redox currents for different CBZ concentrations.

A. Control Amplifier Design

In a 3-electrode CV experiment, a cyclic voltage signal is set across WE and RE, and the resulting current through WE and CE is recorded. As previously mentioned, the first operation of the biosensor is the PEDOT polymerization on the electrode's surface obtained by applying a cyclic potential of -0.1 V to $+1.4$ V across Vcell. Secondly, another CV potential of -0.1 V to $+0.6$ V across Vcell is applied to analyze CBZ levels' effect on the resulting current. Hence, the control amplifier was designed

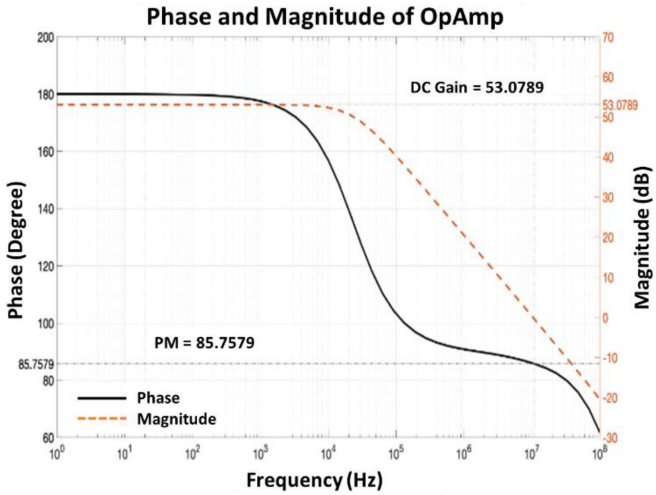

Fig. 6. AC phase margin and gain of the designed Op-Amp.

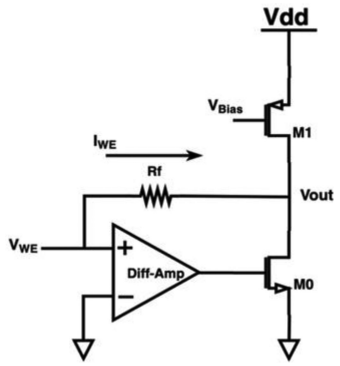

Fig. 7. Transimpedance current to voltage conversion circuit.

to have an input voltage range of −0.0 V to +1.5 V. Another important design factor was the output stage current which limits the flow of current through WE. This current was set to 3 mA to ensure proper operation. Finally, the compliance voltage, which is the maximum voltage required between WE and RE throughout the electrochemical system, was measured in-vitro to be 2 V, therefore it was necessary to minimize the saturation voltages of the output PMOS transistor to obtain 2 V bias between WE and CE.

The control amplifier was designed to be a high gain 2-stage Op-Amp with a power supply of 3.3 V and a bias current of 100 μA. The measured gain was 53.07 dB and with a phase margin of 85.76° as shown in Fig. 6. A 1 pF Miller capacitor was added to ensure stability of the Op-Amp over a wide range of capacitive load.

B. I-V Conversion Circuit

The sensing channel consists of a 2-stage Op-Amp with a feedback resistor in a transimpedance configuration as presented in Fig. 7. The choice of the resistor value is critical to the sensitivity of the sensing amplifier. According to our previous reports, the redox currents could be as high as 800 μA, therefore, the value of Rf was chosen to be 1 kΩ to ensure good sensitivity.

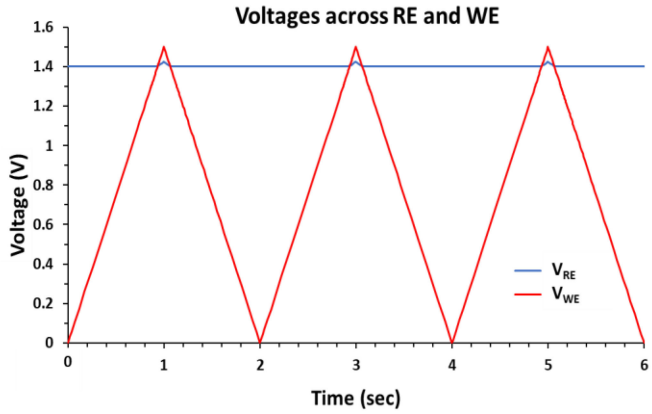

Fig. 8. Recorded potential at WE and RE after applying a cyclic input voltage of −0.0 V to +1.5 V with a step size of 100 mV/s.

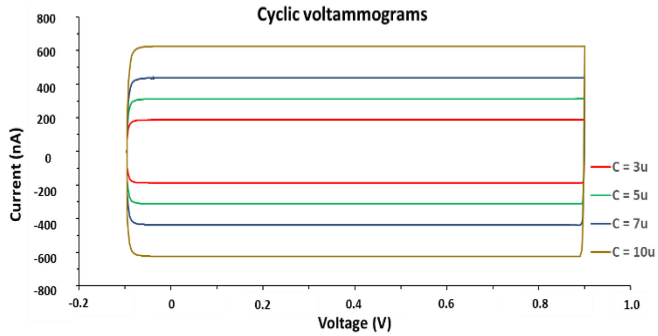

Fig. 9. Electric double layer capacitance plots. Recorded voltammograms of current vs cell voltage with C_{WE} and C_{CE} of 3 uF, 5 uF, 7 uF, and 10 uF.

The −ve terminal of the amplifier was set to ground and the +ve terminal was connected to WE. By applying KCL we obtain.

$$V_{out} - V_{WE} = \frac{I_{WE}}{R_f} \tag{5}$$

$$I_{WE} = \frac{V_{out} - V_{WE}}{R_f} \tag{6}$$

$$I_{WE} = \frac{V_{out} - Vref}{R_f} \tag{7}$$

Since both input terminals of the amplifier have similar voltages due to the high-input impedance, the voltage on WE will become Vref.

A cyclic voltage signal from 0 to 1.5 V with a step size of 100 mV/s was applied at the source of the control amplifier and the voltage Vref was set at 1.4 V which to match Vcell of −0.1 to +1.4 V, which is the maximum voltage required for the polymerization of the imprinted matrix. Afterwards the voltage at WE was measured along with the voltage across RE. Fig. 8 shows that indeed throughout the applied signal, the voltage V_{WE} remained at 1.4 V and V_{RE} was a replica of the source validating successful manipulation of the cell voltage Vcell.

To further test the stability of the potentiostat, the current I_{WE} through the WE was recorded whilst varying C_{CE} and C_{WE} from 1 to 10 μF. The effect of different electric double layer capacitance is provided in Fig. 9.

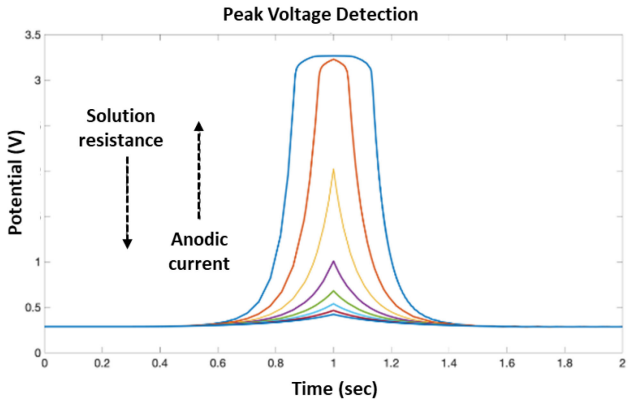

Fig. 10. Peak voltage VR versus solution resistance.

C. Peak Detection Circuit

Peak detection enables us to promptly draw a correlation between CBZ concentration and the anodic peak currents produced. The configuration of the proposed peak detection circuit is provided in Fig. 5. I_{WE} was mirrored through transistors M2 to M3 to the peak detection stage. This current then passes through the resistor R_O. The voltage drop signal across R_O, V_R, is identical in form to that of the redox current I_{WE}. The output resistance value R_O was chosen to be 2 kΩ. The differential amplifier utilized in the current to voltage conversion is similar to the differential amplifier stage in the control Op-Amp with a bias current of 100 μA. Fig. 10 presents the graph of V_R throughout different solution resistance R_S values. As R_S increases the current I_{WE} decreases yielding a decrease in V_R. On the other hand, as R_S decreases, the current I_{WE} increases, yielding an increase in V_R. The same observation could be drawn with respect to changes in the charge transfer resistance R_{ct}.

IV. Experimental Results

This section validates the chip fabrication, the in-vitro setup used to test it, and obtained experimental results. Initially, the fabricated chip was utilized to electropolymerize the molecular imprinted PEDOT on the electrode's surface. Followed by SEM to validate the polymer's formation along with its uniform deposition. Furthermore, CV tests were conducted in order to measure the sensor's response to different therapeutic CBZ levels using $[Fe(CN)_6]^{3-/4-}$ as a redox mediator in PBS. Throughout the experiments, CBZ removal from the imprinted sites was validated through UV-vis spectroscopy.

A. Chip Fabrication

The proposed CMOS biosensor was assembled by Taiwan Semiconductor Manufacturing Company (TSMC), that has a minimum feature size of 0.18 μm and operates at a nominal power supply voltage of 3.3 V. The 1×1 mm^2 chip was packaged and mounted on a socket adapter and then placed on a breadboard for testing. Fig. 11 presents a microscopic image of the fabricated chip along with layout and floorplan consisting of two blocks: the control amplifier and the sense amplifier. The packaged chip

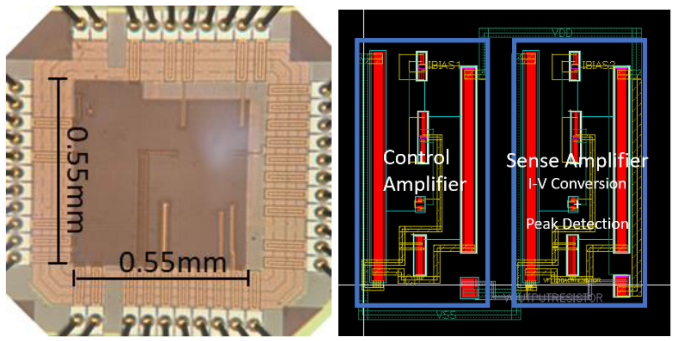

Fig. 11. Photomicrographic image of the fabricated chip along with its layout floorplan.

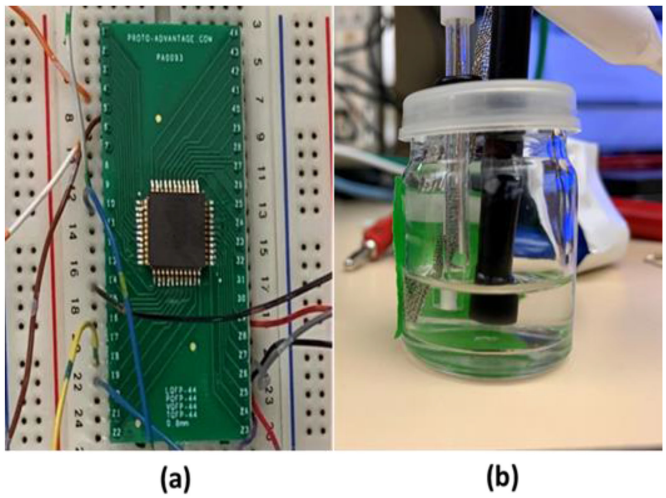

Fig. 12. Test setup (a) packaged chip on adapter socket and breadboard (b) 3-electrode solution testing.

mounted on the adapter socket and the 3-electrode system is shown in Fig. 12.

B. Reagents

CBZ powder along with valproic acid (VPA) and phenytoin (PHT) were supplied by Sigma-Aldrich. All other analytical grade reagents were purchased commercially. The 3,4-Ethylenedioxythiophene (EDOT) monomer was also supplied by Sigma-Aldrich. It was purified by distillation, purged by nitrogen, and stored in darkness at a temperature of 4 °C. PBS was used as the electrolyte. CBZ, VPA and PHT stock solutions were prepared in a mixture of methanol/water (20:80) and stored at a temperature of 4 °C.

C. Test Setup Apparatus

All measurements were conducted in a 3-electrode setup: a molecular imprinted PEDOT modified GCE (MIPEDOT-GCE) (diameter = 2 mm) as the WE; a Pt wire electrode as the CE; and a potassium chloride (KCl)-saturated Ag/AgCl electrode as the RE. A 33210A Keysight Waveform/Function Generator was utilized to apply a CV signal across the cell along with a MDO4104-6 Tektronix mixed domain oscilloscope to probe

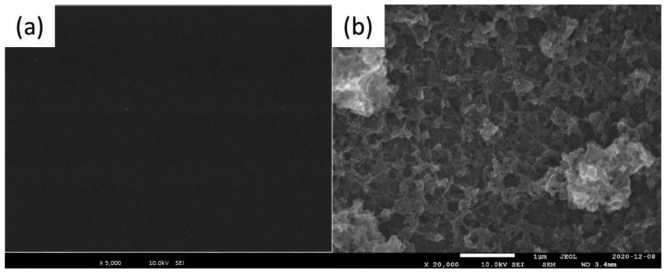

Fig. 13. Surface morphology of (a) bare GCE [23] and (b) electropolymerized PEDOT using SEM at 10 kV and 20000 times magnification.

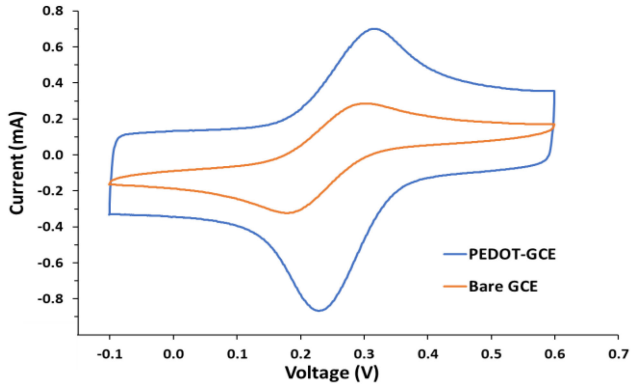

Fig. 14. CV graphs of bare GCE and PEDOT-GCE in PBS solution of 0.01 M $[Fe(CN)_6]^{3-/4-}$ and 0.1 M KCl.

output signals. SEM images were conducted at an electron acceleration voltage of 10 kV.

D. Preparation of CBZ Imprinted PEDOT Films

Prior to use, the bare GCEs were polished using 0.3 μm and 0.05 μm alumina slurry. Afterwards, the electrodes were sonicated in distilled water and ethanol for 5 min each. Furthermore, the GCEs were immersed in an ACN solution containing 0.2 M Bu_4NBF_4, 0.2 M EDOT, and 0.015 M CBZ. PEDOT was electropolymerized to form the imprinted sites on the electrode's surface, a cyclic signal across Vcell with a potential range of -0.1 V to $+1.4$ V and a period of 28 s was applied for a duration of 280 s. The electrodes were then immersed in ACN and stirred constantly for a duration of 30 min. This resulted in the extraction of the CBZ molecules trapped inside polymer matrix. Similarly, non-imprinted PEDOT modified GCEs (NIPEDOT-GCEs) were constructed in absence of CBZ to serve as control electrodes. Fig. 13 provides a SEM image of the MIP post CBZ extraction depicting successful formation of a porous and uniformly deposited structure.

Furthermore, CV measurements portrayed the difference in conductivity of bare GCE's compared to MIPEDOT-GCEs. Hence, a cyclic signal across Vcell with a potential range of -0.1 to $+0.6$ V and a period of 14 s was applied for a duration of 42 s. Fig. 14 provides the recorded cyclic voltammograms.

E. CBZ Extraction Method

The extraction of the CBZ molecules from the imprinted polymer is a main challenge in electropolymerized polymers.

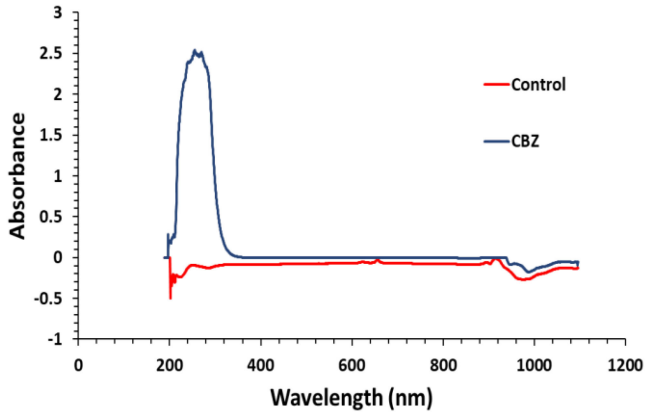

Fig. 15. UV spectra of CBZ in ACN displaying a peak at 230 nm due to the presence of CBZ in solution vs control without the presence of CBZ.

Once exposed to harsh conditions, the polymer on the electrode's surface may be delaminated and lose functionality. Therefore, it is necessary to extract the CBZ molecules in gentler methods. As such, ACN was chosen as the extraction medium since it seamlessly dissolves CBZ. The extraction post-entrapment was conducted through incubating the electrode in ACN and constantly stirring for a period of 30 min. Proper removal of CBZ molecules from the imprinted sites was then validated through performing UV-vis spectroscopy. The UV spectra of the ACN solution utilized for extraction was generated. Fig. 15 illustrates a peak at a wavelength of 230 nm distinct to the presence of CBZ molecules validating the removal of the CBZ molecules from polymer sites.

F. MIPEDOT-GCE Calibration Curve

Therapeutic CBZ concentrations in blood have been reported to be within 4–12 mg/L. Therefore, stock concentrations of 1-50 mg/L of CBZ were prepared by dissolving CBZ in a mixture of methanol/water (20:80). Afterwards the MIPEDOT-GCEs were incubated in the prepared solutions for 15 min with stirring. They were then removed from the solution and left to dry to dry at room temperature. Finally, the electrodes were transferred into a solution of PBS (pH $= 7.4$) containing 0.01 M $[Fe(CN)_6]^{3-/4-}$ and 0.1 M KCl for CV testing. All measurements were conducted 3 times to confirm results validity.

Following a cyclic signal across Vcell with a potential range of -0.1 to $+0.6$ V and a period of 14 s applied for a duration of 42 s, the current peaks were recorded by dividing the voltage drop V_R across the resistor's value. It was observed that the sensor's peak current, equivalent to the maximum current through the solution, had a linear response to CBZ concentration. On the other hand, NIPEDOT-GCEs did not provide a response to CBZ concentration variation. Fig. 16 provides the constructed calibration curve of current variation recorded by the electrode with respect to CBZ concentration. Higher CBZ concentrations inhibited electron transfer at the electrode's surface resulting in a current decrease, hence, a larger current variation with respect to MIPEDOT-GCE response with absence of CBZ.

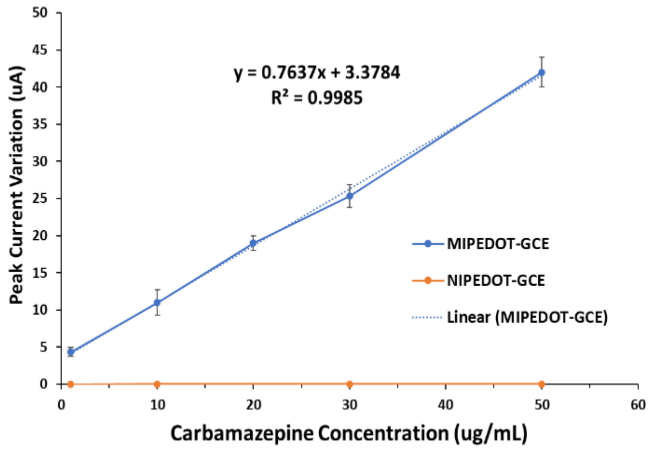

Fig. 16. Calibration curve of peak current variation through modified MIPEDOT and NIPEDOT-GCE versus CBZ concentrations of 0 to 50 ug/mL.

Both Limit of detection (LOD) and limit of Quantification (LOQ) are terms utilized to describe the smallest concentration of the analyte that can be measured. LOD is defined as the lowest concentration that can be detected with a stated probability, although not quantified as an exact value. On the other hand, LOQ is defined as the lowest concentration that can be quantified with a specified acceptable precision and accuracy [25]. The LOD and LOQ were calculated with respect to the linear regression method [26] and found to be 2.04 and 6.2 μg/mL respectively. The biosensor's sensitivity is highly reliant on the CBZ extraction protocol from within the imprinted polymer. Therefore, through the optimization of the extraction protocol, a larger number of CBZ molecules would free up more gaps within the polymer and enhance detection. Additionally, sensitivity may be enhanced through increasing the conductivity and surface area of the polymer. The latter can be accomplished by adding conductive graphene to the mixture.

G. Selectivity Tests

To test the selectivity of the fabricated sensor, we studied the sensor's response to two competing ASMs. Both PHT and VPA are routine ASMs which may be prescribed along with CBZ. Their therapeutic levels have been established to be 10–20 μg/mL and 50–125 μg/mL respectively [27]. As such stock solutions of PHT and VPA were prepared by dissolving each drug in a methanol/water mixture (20:80). Concentrations were chosen to be with 1-150 μg/mL to cover a range wider than what has been therapeutically reported. Furthermore, the MIPEDOT-GCEs were incubated in each stock solution followed by constant stirring for 15 min. The electrodes were then left to dry before transferring them into a solution of PBS (pH = 7.4) containing 0.01 M $[Fe(CN)_6]^{3-/4-}$ and 0.1 M KCl for CV testing. After applying a cyclic signal across Vcell with a potential range of -0.1 to $+0.6$ V and a period of 14 s applied for a duration of 42 s, no peak current change was measured. This confirms that the fabricated sensor is not influenced by drugs other than CBZ rendering it selective solely to CBZ.

TABLE I
COMPARISON WITH RECENT CBZ ELECTROCHEMICAL-BASED DETECTION SENSORS

Material	Method	LOD	Sel.	Ref
GO-g-C3N4	Amp.	10.5 nM	No	[6]
NiSe2	Amp.	18.2 nM	No	[28]
Au@AgPdNPs -β-CD-IL/GCE	CV	0.089 µM	No	[29]
Ce-ZnO/rGO/GCE	DPV	1.2 nM	No	[30]
MIPEDOT-GCE	CV	8.6 µM	**Yes**	This work

LOD, limit of detection Sel, selectivity

H. Stability Tests

Stability of the fabricated MIP electrodes was studied by recording their redox peak currents in a PBS solution containing 0.01 M $[Fe(CN)_6]^{3-/4-}$ and 0.1 M KCl while applying a cyclic cell voltage of -0.1 to $+0.6$ V with a period of 14 s for 42 s. Throughout a duration of 2 months, the electrodes showed no noticeable decline in performance and their respective peak currents remained constant.

I. Proposed Sensor's Advantages

Table I summarizes the most recent CBZ detection sensors based on electrochemical methods. Sensors are classified based on their selectivity and sensitivity and must possess both attributes in order to successfully target a molecule within a complex medium. Compared to the existing sensors, the proposed sensor is the only sensor capable of selective detection of CBZ, rendering it the most effective in complex media. Despite their superior sensitivity, existing sensors lack selectivity and therefore suffer from interfering drugs or substances. Additionally, another advantage of the proposed sensor is its ability to be tailored towards the detection of various drugs. This can be achieved by using another drug as a template while imprinting the PEDOT polymer. Hence, the proposed sensor is not limited to the detection of CBZ but potentially a wider variety of ASMs.

J. Future Work and Limitations

In the present study, a simplified architecture potentiostat was implemented for electrochemical measurements. However, signal to noise ratio and sensitivity could be greatly improved by using a differential potentiostat topology as suggested in [31] along with proper offset cancelation [32]. Additionally, the use of a multichannel potentiostat [33] would enable concurrent measurements and greatly reduce measurement time whilst enhancing sensitivity and sensor's performance.

Furthermore, the use of integrated electrodes may greatly improve signal to noise ratio by eliminating the effect of connectors thus enhancing sensors sensitivity. Along with that, it is of great importance to optimize the CBZ extraction protocol liberating more imprinted sites for better template removal.

V. Conclusion

The presented biosensor is intended for the therapeutic drug monitoring of patients with epilepsy through the electropolymerization of molecular imprinted PEDOT on GCEs, and the successful detection and quantification of CBZ molecules. It is composed of a TSMC180nm CMOS chip coupled with a 3-electrode electrochemical cell. The circuit operates at a nominal supply voltage of 3.3 V and is capable of performing CV required for both PEDOT polymerization and CBZ detection. A cyclic input signal with a potential range of 0 to +1.4 V with a period of 28 s applied for 280 s successfully polymerized molecular imprinted PEDOT on the GCE's surface. This was validated by SEM images presenting the uniform deposition and porous morphology of the polymer.

Furthermore, a cyclic input signal with a potential range of −0.1 to +0.6 V with a period of 14 s applied for 42 s triggered the redox currents of the mediator pair $[Fe(CN)_6]^{3-/4-}$ enabling the successful quantification of CBZ molecules entrapped within the polymer matrix. The LOD and LOQ of the biosensor were found to be 2.04 and 6.2 μg/mL respectively. These values are superior to our previously reported values of 231.5 and 791.0 μg/mL respectively [21]. Additionally, the sensors selectivity was validated by incubation in PHT and VPA. No response due to such incubation was measured. Further sensor optimization could be done by integrating the electrodes withing the chip, enabling multi-channel detection, and enhancing the potentiostat's performance by increasing its signal-to-noise ratio.

Acknowledgment

The authors would like to thank Canada for funding the research, along with Dr. Steen B. Schougaard for offering access to his facilities.

References

[1] R. D. Thijs, R. Surges, T. J. O'Brien, and J. W. Sander, "Epilepsy in adults," *Lancet*, vol. 393, no. 10172, pp. 689–701, 2019.

[2] S. L. Moshé, E. Perucca, P. Ryvlin, and T. Tomson, "Epilepsy: New advances," *Lancet*, vol. 385, no. 9971, pp. 884–898, 2015.

[3] N. Lavanya *et al.*, "A novel disposable electrochemical sensor for determination of carbamazepine based on fe doped SnO_2 nanoparticles modified screen-printed carbon electrode," *Mater. Sci. Eng.: C*, vol. 62, pp. 53–60, 2016.

[4] S. Z. Mohammadi, T. Rohani, A. Beheshti, and M. Dadkhodazadeh, "Molybdenum disulfide/graphene oxide nanohybrid as an electrocatalyst for sensitive detection of carbamazepine in human body fluid samples," *Iranian J. Anal. Chem.*, vol. 8, no. 1, pp. 87–92, 2021.

[5] M. Pierpaoli *et al.*, "Simultaneous opto-electrochemical monitoring of carbamazepine and its electro-oxidation by-products in wastewater," *J. Hazardous Mater.*, vol. 419, 2021, Art. no. 126509.

[6] P. Balasubramanian *et al.*, "An amperometric sensor for low level detection of antidepressant drug carbamazepine based on graphene oxide-g-C3N4 composite film modified electrode," *J. Electrochem. Soc.*, vol. 165, no. 3, 2018, Art. no. B160.

[7] B. Unnikrishnan, V. Mani, and S.-M. Chen, "Highly sensitive amperometric sensor for carbamazepine determination based on electrochemically reduced graphene oxide–single-walled carbon nanotube composite film," *Sensors Actuators B: Chem.*, vol. 173, pp. 274–280, 2012.

[8] N. M. Mansour, D. T. El-Sherbiny, F. A. Ibrahim, and H. I. El Subbagh, "Development of an inexpensive, sensitive and green HPLC method for the simultaneous determination of brivaracetam, piracetam and carbamazepine; application to pharmaceuticals and human plasma," *Microchemical J.*, vol. 163, 2021, Art. no. 105863.

[9] A. A. Hassan, A. Tanimu, and K. Alhooshani, "Iron and cobalt-containing magnetic ionic liquids for dispersive micro-solid phase extraction coupled with HPLC-DAD for the preconcentration and quantification of carbamazepine drug in urine and environmental water samples," *J. Mol. Liquids*, vol. 336, 2021, Art. no. 116370.

[10] H. Heidari and B. Yari, "Multivariate optimization of an ultrasound-assisted deep eutectic solvent-based liquid-phase microextraction method for HPLC–UV analysis of carbamazepine in plasma," *Chromatographia*, vol. 83, no. 12, pp. 1467–1475, 2020.

[11] H. Deepakumari and H. Revanasiddappa, "Development and validation of a uvspectrophotometric method for the quantitative determination of oxcarbazepine and study of its degradation profile," *Chem. Sci. J.*, vol. 5, 2014, Art. no. 1.

[12] B. Liu, D. Tang, B. Zhang, X. Que, H. Yang, and G. Chen, "Au (III)-promoted magnetic molecularly imprinted polymer nanospheres for electrochemical determination of streptomycin residues in food," *Biosensors Bioelectron.*, vol. 41, pp. 551–556, 2013.

[13] G. Cai, Z. Yu, and D. Tang, "Actuating photoelectrochemical sensing sensitivity coupling core-core-shell Fe_3O_4@ C@ Tio_2 with molecularly imprinted polypyrrole," *Talanta*, vol. 219, 2020, Art. no. 121341.

[14] H. Karimi-Maleh *et al.*, "A novel detection method for organophosphorus insecticide fenamiphos: Molecularly imprinted electrochemical sensor based on core-shell Co_3O_4@ MOF-74 nanocomposite," *J. Colloid Interface Sci.*, vol. 592, pp. 174–185, 2021.

[15] M. Beytur *et al.*, "A highly selective and sensitive voltammetric sensor with molecularly imprinted polymer based silver@ gold nanoparticles/ionic liquid modified glassy carbon electrode for determination of ceftizoxime," *J. Mol. Liquids*, vol. 251, pp. 212–217, 2018.

[16] M. L. Yola and N. Atar, "Development of molecular imprinted sensor including graphitic carbon nitride/N-doped carbon dots composite for novel recognition of epinephrine," *Composites Part B: Eng.*, vol. 175, 2019, Art. no. 107113.

[17] N. Özcan, H. Medetalibeyoglu, O. Akyıldırım, N. Atar, and M. L. Yola, "Electrochemical detection of amyloid-β protein by delaminated titanium carbide MXene/multi-walled carbon nanotubes composite with molecularly imprinted polymer," *Mater. Today Commun.*, vol. 23, 2020, Art. no. 101097.

[18] C. Bodart *et al.*, "Electropolymerized poly (3, 4-ethylenedioxythiophene) (PEDOT) coatings for implantable deep-brain-stimulating microelectrodes," *ACS Appl. Mater. Interfaces*, vol. 11, no. 19, pp. 17226–17233, 2019.

[19] R. Zeng *et al.*, "CRISPR-Cas12a-driven MXene-PEDOT: PSS piezoresistive wireless biosensor," *Nano Energy*, vol. 82, 2021, Art. no. 105711.

[20] L. Huang, Z. Yu, J. Chen, and D. Tang, "Pressure-based bioassay perceived by a flexible pressure sensor with synergistic enhancement of the photothermal effect," *ACS Appl. Bio Mater.*, vol. 3, no. 12, pp. 9156–9163, 2020.

[21] A. Hammoud, D. Chhin, D. Nguyen, and M. Sawan, "A new molecular imprinted PEDOT glassy carbon electrode for carbamazepine detection," *Biosensors Bioelectron.*, vol. 180, 2021, Art. no. 113089.

[22] Y. Koç, U. Morali, S. Erol, and H. Avci, "Investigation of electrochemical behavior of potassium ferricyanide/ferrocyanide redox probes on screen printed carbon electrode through cyclic voltammetry and electrochemical impedance spectroscopy," *Reactions*, vol. 14, p. 15, 2021.

[23] B. Chen *et al.*, "Penetrating glassy carbon neural electrode arrays for brain-machine interfaces," *Biomed. Microdevices*, vol. 22, pp. 1–10, 2020.

[24] M. M. Ahmadi and G. A. Jullien, "Current-mirror-based potentiostats for three-electrode amperometric electrochemical sensors," *IEEE Trans. Circuits Syst. I: Regular Papers*, vol. 56, no. 7, pp. 1339–1348, Jul. 2009.

[25] D. W. Tholen*et al.*, "Protocols for determination of limits of detection and limits of quantitation; approved guideline." *CLSI EP17-A*, vol. 24, p. 34, 2004.

[26] A. Shrivastava and V. B. Gupta, "Methods for the determination of limit of detection and limit of quantitation of the analytical methods," *Chronicles Young Scientists*, vol. 2, no. 1, pp. 21–25, 2011.

[27] A. Jain, I. Haque, V. Tayal, and V. Roy, "Valproic acid-induced acute pancreatitis," *Indian J. Psychiatry*, vol. 61, no. 4, 2019, Art. no. 421.

[28] S. Veeralingam and S. Badhulika, "Two-dimensional metallic $NiSe_2$ nanoclusters–based low-cost, flexible, amperometric sensor for detection of neurological drug carbamazepine in human sweat samples," *Front. Chem.*, vol. 8, 2020, Art. no. 337.

[29] L. Daneshvar and G. H. Rounaghi, "An electrochemical sensing platform for carbamazepine determination based on trimetallic Au-Ag-Pd dendritic nanopatricles, supramolecular β-cyclodextrin and [bmim] NTF2 ionic liquids," *J. Electrochem. Soc.*, vol. 164, no. 6, 2017, Art. no. B177.

[30] N. Dhanalakshmi, T. Priya, and N. Thinakaran, "Highly electroactive Ce-ZnO/rGO nanocomposite: Ultra-sensitive electrochemical sensing platform for carbamazepine determination," *J. Electroanal. Chem.*, vol. 826, pp. 150–156, 2018.

[31] S. Subhan, S. Khapli, Y.-A. Song, and S. Ha, "A fully differential potentiostat circuit with integrated time-based ADCs," in *Proc. IEEE Biomed. Circuits Syst. Conf.*, 2019, pp. 1–4.
[32] M. Duwe and T. Chen, "Low power integrated potentiostat design for μ electrodes with improved accuracy," in *Proc. IEEE 54th Int. Midwest Symp. Circuits Syst.*, 2011, pp. 1–4.
[33] G. Massicotte, S. Carrara, G. Di Micheli, and M. Sawan, "A CMOS amperometric system for multi-neurotransmitter detection," *IEEE Trans. Biomed. Circuits Syst.*, vol. 10, no. 3, pp. 731–741, Jun. 2016.

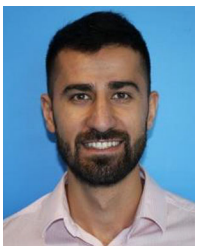

Abbas Hammoud (Student Member, IEEE) was born in Beirut, Lebanon, in 1989. He received the B.Sc. degree (with distinction) in computer engineering from Concordia University, Montreal, QC, Canada, in 2014. He was the recipient of a research award fund where he commenced his research in analog/mixed-signals. He was granted a direct passage from a bachelor's degree towards obtaining a Ph.D. degree in electrical engineering with the Polystim Neurotechnologies Laboratory at Polytechnique Montreal, Montreal. His main research interests include the design of analog/mixed-signal integrated circuits for biosensors and lab-on-chip applications.

Hussein Assaf received the B.E. and M.E. degrees in electrical and computer engineering from the American University of Beirut (AUB), Beirut, Lebanon, in 2011 and 2013, respectively, with emphasis on Security. Between 2011 and 2013, he was a Research Assistant with AUB and was a Member of the NetSecReasearch.org Group, AUB. He was also a Lab Instructor with AUB (Fall 2013) and with Arts Sciences and Technology University in 2015. In 2016, Hussein joined POLYSTIM as a Ph.D. candidate with Polytechnique Montreal.

Yvon Savaria (Fellow, IEEE) received the B.Ing. and M.Sc.A degrees in electrical engineering from École Polytechnique Montreal, Montréal, QC, Canada, in 1980 and 1982, respectively, and the Ph.D. degree in electrical engineering from McGill University, Montreal, in 1985. Since 1985, he has been with Polytechnique Montréal, where he is currently a Professor with the Department of Electrical Engineering. He is also affiliated with the Hangzhou Innovation Institute of Beihang University, Beijing, China. He has carried out work in several areas related to microelectronic circuits and microsystems, such as testing, verification, validation, clocking methods, defect and fault tolerance, effects of radiation on electronics, high-speed interconnects and circuit design techniques, CAD methods, reconfigurable computing and applications of microelectronics to telecommunications, aerospace, image processing, video processing, radar signal processing, and the acceleration of digital signal processing. He is currently involved in several projects related to embedded systems in aircrafts, radiation effects on electronics, asynchronous circuit design and testing, green IT, wireless sensor networks, virtual networks, software-defined networks, machine learning, embedded ML, computational efficiency and application-specific architecture design. He holds 16 patents, has authored or coauthored 180 journal papers and 480 conference papers, and was the thesis advisor of 170 graduate students who completed their studies.

He was the Program Co-Chairman of NEWCAS'2018 and the General Chairman of NEWCAS'2020. He has been working as a consultant or was sponsored for carrying out research with Bombardier, Buspass, CNRC, Design Workshop, Dolphin, DREO, Ericsson, Genesis, Gennum, Huawei, Hyperchip, Intel, ISR, Kaloom, LTRIM, Miranda, MiroTech, Nortel, Octasic, PMC-Sierra, Space codesign, Technocap, Thales, Tundra, and Wavelite. He is a Member of the executive committee of the Regroupement Stratégique en Microélectronique du Québec (RESMIQ) and a Member of the Ordre des Ingénieurs du Québec (OIQ), and he is a Member of the CMC Microsystems Technical Advisory committee. In 2001, he was awarded a Tier 1 Canada Research Chair on the designs and architectures of advanced microelectronic systems that he held until June 2015. He was the recipient of the Synergy Award of the Natural Sciences and Engineering Research Council of Canada in 2006. Since June 2019, he has been the NSERC-Kaloom-Intel-Noviflow (KIN) Chair professor.

Dang Khoa Nguyen is currently a Neurologist with Montreal University Health Center (CHUM), Clinician Scientist with the CHUM Research Center, a Professor with the Department of Neurosciences, University of Montreal, and immediate past-president of the Canadian League against Society. He is currently holds a Canadian Institutes of Health Research Chair in Epilepsy.

Mohamad Sawan (Fellow, IEEE) received the Ph.D. degree from the University of Sherbrooke, Sherbrooke, QC, Canada. He is currently a Chair Professor with Westlake University, Hangzhou, China, and Emeritus Professor with Polytechnique Montreal, Montréal, QC, Canada. He is a Founder and the Director of the Cutting-Edge Net of Biomedical Research And INnovation (CenBRAIN), Westlake University, Hangzhou, China. He has authored or coauthored more than 800 peer reviewed papers, two books, ten book chapters, and 12 patents. He is a Co-Founder, an Associate Editor and was the Editor-in-Chief of the IEEE TRANSACTIONS ON BIOMEDICAL CIRCUITS AND SYSTEMS during 2016–2019. He is the Founder of the Polystim Neurotech Laboratory, and a Co-Founder of the International IEEE-NEWCAS and International IEEE-BioCAS Conference. He was the General Chair of the 2020 IEEE International Medicine, Biology and Engineering Conference (EMBC). He was awarded the Canada Research Chair in Smart Medical Devices (2001–2015), and was leading the Microsystems Strategic Alliance of Quebec, Canada (1999–2018). He was the recipient of several awards, including the Queen Elizabeth II Golden Jubilee Medal, Shanghai International Collaboration Award, Qianjiang Friendship Ambassador Award, and Medal of Merit from the President of Lebanon. Dr. Sawan is a Fellow of the Canadian Academy of Engineering, Fellow of the Engineering Institutes of Canada, and "Officer" of the National Order of Quebec.